AIP Advances

Dielectric barrier discharge actuator for vehicle drag reduction at highway speeds

Subrata Roy, Pengfei Zhao, Arnob DasGupta, and Jignesh Soni

Citation: AIP Advances **6**, 025322 (2016); doi: 10.1063/1.4942979
View online: http://dx.doi.org/10.1063/1.4942979
View Table of Contents: http://scitation.aip.org/content/aip/journal/adva/6/2?ver=pdfcov
Published by the AIP Publishing

Dielectric barrier discharge actuator for vehicle drag reduction at highway speeds

Subrata Roy,[a] Pengfei Zhao, Arnob DasGupta, and Jignesh Soni
Applied Physics Research Group, Department of Mechanical & Aerospace Engineering, University of Florida, Gainesville, Florida 32611, USA

(Received 11 June 2015; accepted 16 February 2016; published online 24 February 2016)

We propose and demonstrate reduction of aerodynamic drag for a realistic geometry at highway speeds using serpentine dielectric barrier discharge actuators. A comparable linear plasma actuator fails to reduce the drag at these speeds. Experimental data collected for linear and serpentine plasma actuators under quiescent operating conditions show that the serpentine design has profound effect on near wall flow structure and resulting drag. For certain actuator arrangement, the measured drag reduced by over 14% at 26.8 m/s (60 mph) and over 10% at 31.3 m/s (70 mph) opening up realistic possibility of reasonable energy savings for full scale ground vehicles. In addition, the power consumption data and drag reduction effectiveness for different input signals are also presented. [http://dx.doi.org/10.1063/1.4942979]

I. INTRODUCTION

The presence of aerodynamic drag limits the fluid dynamic performance of any vehicle. For example, the aerodynamic drag may comprise upwards of 50%, 65% and 70% of the total drag for commercial air vehicles, heavy highway vehicles and high speed trains, respectively.[1] Hence, any method for reducing this drag, including but not limited to controlling surface receptivity and fluidic actuation, can have profound influence in transportation applications.[2] Ever since its first reported success,[3] plasma actuators have been extensively investigated for improving authority of flow control but with limited success due to their inherent near wall momentum/heat injection method. Such actuators produce a high gradient at the wall limiting an effective control. Efforts have also been invested in influencing the drag, specifically turbulent drag, using plasma actuators.[4]

Specifically, the standard straightedge dielectric barrier discharge (DBD) actuator employs an exposed electrode and an asymmetrically displaced encapsulated electrode to generate a directional plasma body force due to the surface discharge. The power budget associated with these actuators is 10-100 watts per meter length of the actuator. As the discharge expands along the dielectric surface, momentum is transferred from ions in plasma to the surrounding fluid, generating a Glauert-like "wall jet" very close to the work surface. This wall jet also produces a large streamwise velocity gradient and a resulting roll-up streamwise vortex structure downstream of the actuator far beyond the encapsulated electrode resulting in an interaction with the neighboring flow. This wall jet has been widely investigated for momentum addition applications,[5] such as flow separation control over airfoils[6] and turbine blades,[7] and for boundary layer manipulation.[8] Various parametric studies have focused on increasing the velocity and momentum transfer of this wall jet.[9–11] The capability of such actuators is often quantified by the velocity ratio, which is the ratio of the induced jet velocity to the velocity of the bulk flow, and is limited by their associated skin friction drag. In fact, application of standard actuator for drag reduction at lower velocities may be counterproductive as the induced wall jet introduces more wall shear. The challenge is even more daunting at higher velocities (and velocity ratios) when the influence of induced wall jet and a majority one-dimensional vortical structure fails to control the flow streaks.

[a]Electronic mail: roy@ufl.edu. URL: http://aprg.mae.ufl.edu/roy/.

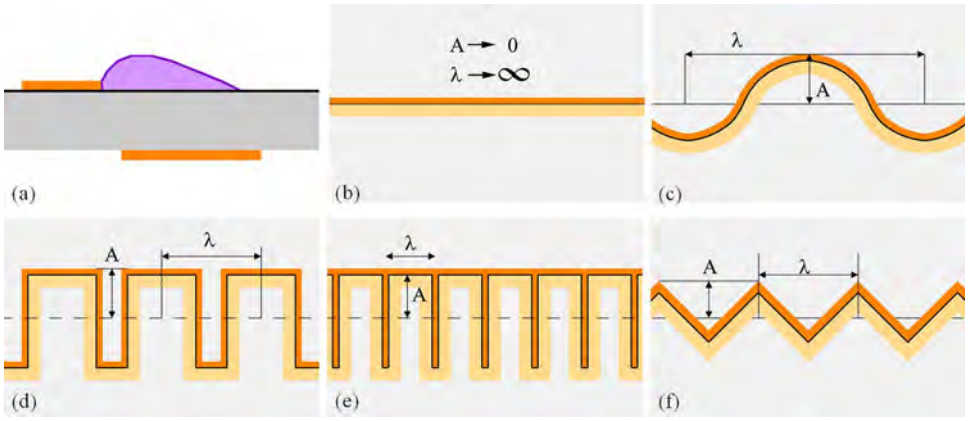

FIG. 1. (a) Schematic of DBD plasma actuator and the generated body force. (b) Linear, (c) arc, (d) rectangle, (e) comb/finger, and (f) triangle geometry serpentine actuators. Reproduced with permission from J. Appl. Phys. 114, 083303 (2013). Copyright 2013 AIP Publishing LLC.

Contrarily for a serpentine actuator, the induced flow is vectored at an angle away from the surface and due to simultaneous pinching and spreading effects on the neighboring flow a fully three-dimensional vortical structure rapidly turbulizes the flow, thickening the boundary layer.[12–14] The general shapes of serpentine actuator are shown in Fig. 1 (taken from Ref. 14). An interesting outcome of such actuation is the capability of introducing periodic hairpins and possibly controlling the flow streaks by changing the wavelength and/or the amplitude of the serpentine geometry.[14,15]

Based on the numerical results,[14] serpentine actuators can induce momentum transport in wall turbulence. This begins with near-wall quasi-streamwise vortices in the buffer layer producing hairpin vortices that auto-generate to produce packets of hairpins containing long, low-momentum zones in the logarithmic layer with and without the influence of thermal energy addition. Evidence indicates that substantial drag reduction is accomplished if the auto-generation mechanism is disrupted or inhibited by weakening the hairpin legs.[16] Stimulation of small scales by plasma actuators may find its heightened effects when keyed to the large-scale motions. By knowing which perturbations will be most amplified, the geometry and operation of the actuators (i.e. flow control devices) can be tailored specifically to excite modes for maximal flow control. This results in a useful control mechanism for aerodynamic drag for which the traditional actuators fails to show any beneficial effect.

Specifically for three-dimensional tractor-trailer geometry, the drag is almost equally distributed into the frontal drag (~25%), skin friction and gap drag (~20%) along large flat surfaces and between tractor and the trailer, under carriage drag underneath the trailer body (~30%) and the wake drag behind the trailer (~25%).[17] Of these, the majority (over 90%) is due to pressure drag from inertial changes. The skin friction drag over the large open surfaces of the truck is less than 10%.[18] For example, the US Class 8 semi-truck with 18 wheels has large frontal area and a complicated under carriage design that create significant drag. It also has a box-like trailer designed to maximize cargo space. This causes a large pressure drag from the trailing wake region resulting in a huge fuel penalty.[19] While streamlining the frontal area and applying skirt around the under carriage helps reducing the frontal and under carriage drag, respectively, the wake drag behind the trailer remains a challenge for drag reduction.

II. EXPERIMENTAL SETUP

We introduce the serpentine class of dielectric barrier discharge actuator[12–15] for effectively modifying aerodynamic drag for three-dimensional vehicle geometry. Specifically, this paper aims to demonstrate drag reduction of a 1:60 scale tractor-trailer truck model at highway speeds of 60 and 70 mph (26.8 and 31.3 m/s, respectively). Based on the geometry of the vehicle, the flow is

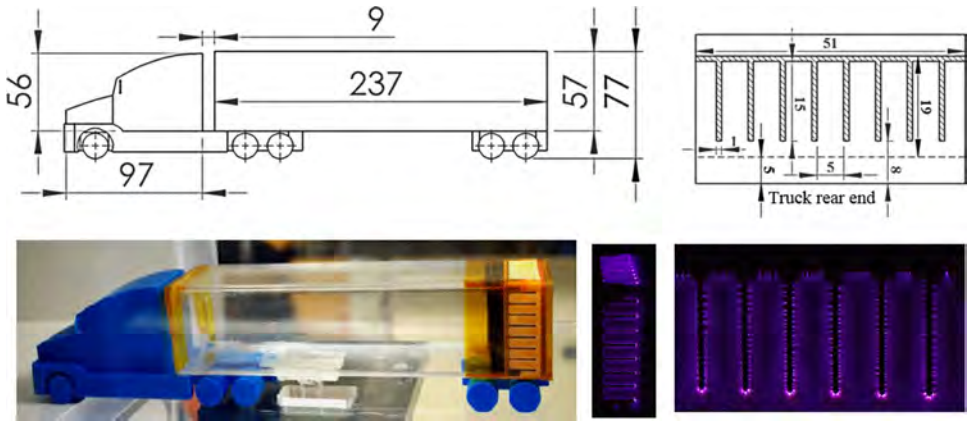

FIG. 2. Tractor-trailer truck 1:60 scale model with serpentine plasma actuator. The truck is 57 mm wide. All dimensions are in mm.

turbulent at these velocities. We note that recent reports on plasma actuation show various levels of success for flow control. For example, in a 1.75 m/s flow over a flat plate the skin friction drag has been estimated to reduce by up to 45% by inducing spanwise oscillation and spanwise travelling wave using plasma actuators.[20] For flow over a backward facing step geometry the influence of flow actuation on the Reynolds stress has also been reported using standard linear plasma actuator (under 15 m/s)[21] and serpentine actuator (under 20 m/s).[22] However, all these experiments were done at low flow speeds over relatively simple geometries. For realistic vehicle geometry, wake drag also plays a major role in overall aerodynamic drag. Higher vehicle speed thus severely limits the control authority of any actuator. To our knowledge, successful demonstration of vehicular drag reduction using plasma actuators at highway speeds has not yet been reported.

For our experiments, we use an open circuit low speed wind tunnel with a cross-section of 305 mm × 305 mm. The length of the test section is 610 mm. The truck dimensions, actuator location, and the truck model inside wind tunnel are shown in Figure 2. The front end of the truck is placed around 38 mm inside the nozzle leaving around 380 mm after the truck. The total aerodynamic drag from skin friction and pressure is measured directly using two-axes dynamometer and only the drag data (force along streamwise direction) is collected. Two Shaevitz Sensors LVDT voltage modules are used to record the lift and drag with a precision of 5 mN. The analog output from the dynamometer is read using a LabVIEW interface.

Both straightedge "linear" actuator and serpentine actuator are investigated for drag reduction. In both cases, the encapsulated electrodes are made from a 60 μm copper tape, and the dielectric materials used are 3.175 mm thick acrylic. The dimensions for this actuator is given in Fig. 2. For the linear actuator the exposed electrode is made from a 60 μm thick adhesive backed copper tape. For serpentine actuator, the exposed electrode pattern (Fig. 2, upper right) is fabricated using photolithography on a Kapton tape with a thickness of 500 nm to ensure high fidelity of the device. In both cases, a 50 μm thick Kapton tape is used on the upstream edge of the exposed electrode to prevent reverse discharge, as well as to encapsulate the grounded electrode. These actuators are placed on the top and side surfaces with the ground electrode 5 mm from the trailing edge of the truck (see Fig. 2). The serpentine actuator geometry is similar to that described in Fig. 1(e) with wavelength λ = 5 mm and amplitude A = 7.5 mm.

The fluid-thermal performances of these actuators are tested in a quiescent chamber (0.61 × 0.61 × 1.22 m) where the bulk flow is negligible and the actuator is running in continuous mode. The test is performed using a particle image velocimetry (PIV) system and an infrared (IR) imaging system. A Phantom v7.3 high speed camera in combination with a 105 mm macro-lens was employed to capture PIV images. The camera was aligned perpendicular to the laser light sheet with a distance of 0.5 m. The field of view captured for each image was approximately 45 × 60 mm. The light sheet cutting the actuators was generated using a Nd : YAG dual cavity pulsed 532nm laser (New Wave Research Solo PIV II 30). Seeding for PIV was generated by a TSI atomizer

(Model 9302) with Ondina oil. When atomizer was pressurized at 25 psi, the mean diameter of the oil droplet is about 0.8 μm.[12] DaVis 7.2 imaging and post processing software was used to capture and analyze PIV images. A FLIR A325 camera with standard built-in 25° lens was employed to capture the IR temperature image of the actuator. LabVIEW codes were utilized to record force, peak-to-peak voltage and current measurements from a Tektronix DPO3014 oscilloscope. This model has a maximum sampling rate of 2.5 GSa/s at a bandwidth of 100 MHz. Voltage is measured using a Tektronix (Model P6015A) passive probe having an attenuation of 1000x. The frequency response of the probe is able to measure AC voltages up to 40 kV with a rated accuracy of ± 3%. Current is measured with a Pearson Electronics (Model 2100) inductive coil type current probe. This probe has a manufacturer rated accuracy of ± 1% and a 20MHz bandwidth. A sinusoidal output signal generated in a Tektronix arbitrary function generator (Model AFG3022B) is passed through a QSC audio amplifier (Model RMX 2450), and then through a custom Corona Magnetics Inc. high voltage transformer to step up the voltage to the desired levels.

III. RESULTS AND DISCUSSION

The PIV experiments are performed in quiescent chamber to elucidate the difference between the two distinct types of actuators, namely, the linear actuator with straight edge and the serpentine actuator with comb like fingers. The result for the linear actuator plotted in Fig. 3(a) shows a known wall jet pattern that expands slightly due to the backward step at the trailing edge. The induced velocity (majorly streamwise) is about 3.5 m/s at 24 kV_{pp} and 5 kHz. The difference between the standard linear and the comb-shaped serpentine design is clearly demonstrated in Fig. 3(b)-3(c). The periodic finger structure allows pinching and spreading of the neighboring fluid rapidly inducing three-dimensional vortices similar to previously reported results.[12,14] Distinctly, the flow field between the fingers demonstrates the effect of pinching in Fig. 3(b) and that of spreading in Fig. 3(c). Note that both these effects are somewhat modified by the presence of the backward step. However, a quick comparison between Fig. 3(a) and Fig. 3(b) shows a larger vertical spreading due to serpentine actuation downstream of the truck trailing edge. This indicates that serpentine actuator should have a stronger influence in the wake region of the truck. Note that the average error considering both statistical and device error for PIV result is about 5%.

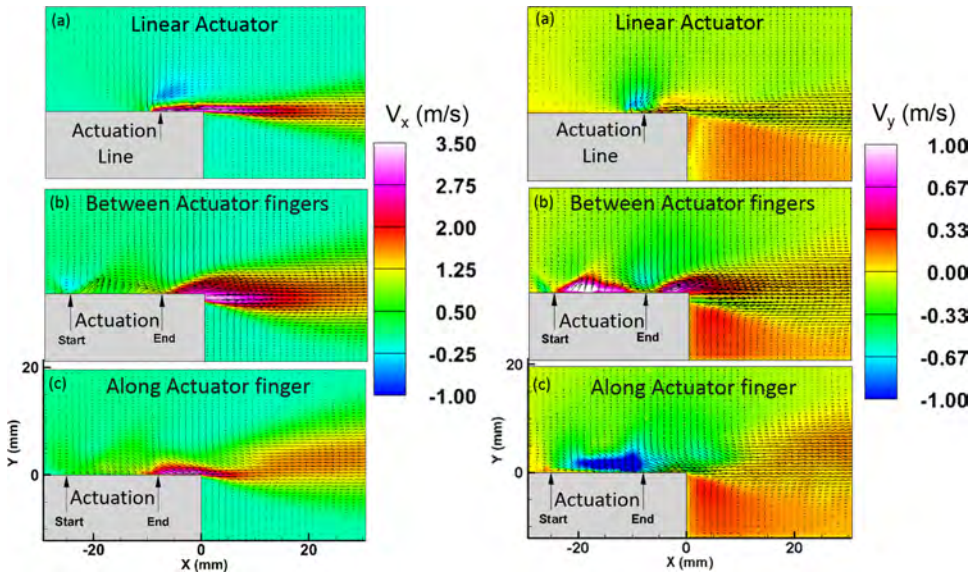

FIG. 3. PIV test result comparison for near field flow inducement along the streamwise plane under quiescent condition shows the streamwise (V_x) and normal (V_y) velocity components. (a) Linear, (b) Serpentine between fingers, (c) Serpentine along the finger.

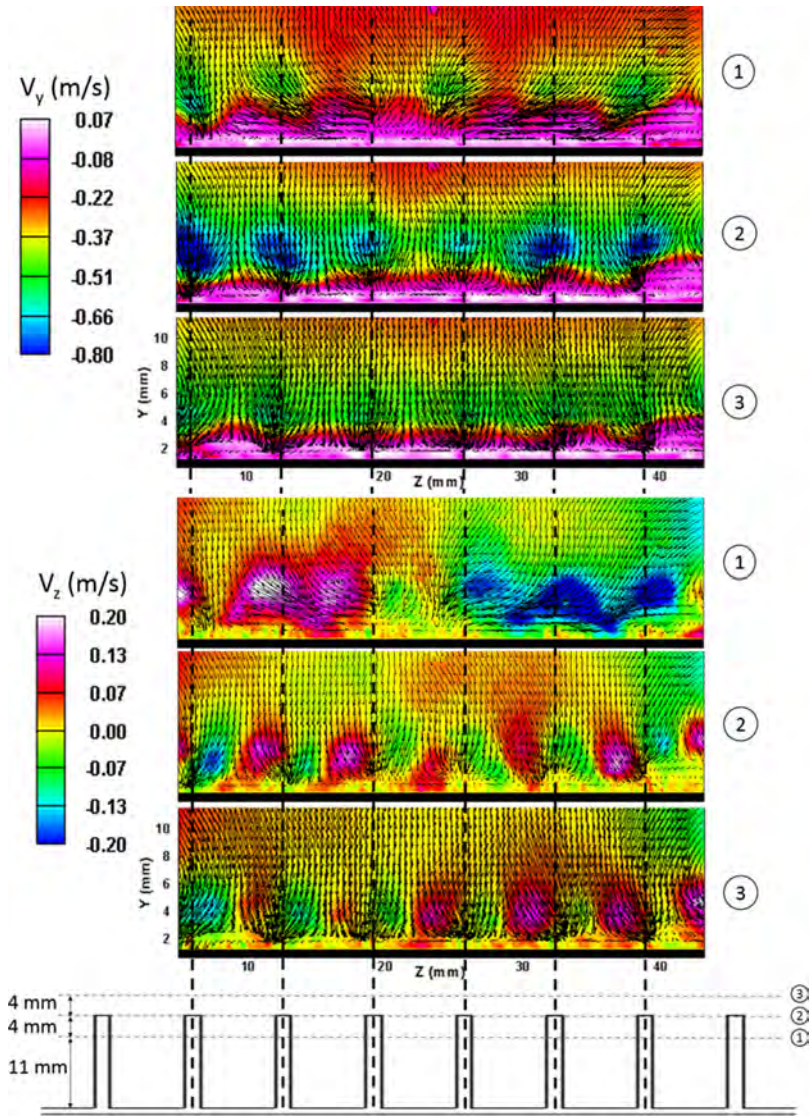

FIG. 4. PIV test result for near field flow inducement along the spanwise plane under quiescent condition shows the normal (V_y) and spanwise (V_z) velocity components. 1, 2 and 3 denote the cross-sectional planes where the PIV measurements were carried out.

PIV measurements are also done along three spanwise cross-sections. These are depicted in Fig. 4. The vectors in these figures are constructed using three times the spanwise velocity v_z and the normal velocity v_y. This is done to clearly describe the pinching and spreading effects[12] generated by the actuator. It shows that there is strong pinching effect at the fingers and spreading effect between them. This is unlike the circular serpentine actuators[12] where the flow is pushed up at the pinching location and accelerated forward in the spreading location. This is due to the fact that the pinching location is really small (finger thickness 2 mm) which does not allow room for the flow to be lifted. Thus the upward momentum created between the finger structures balance the momentum created by the downward pinching force at finger locations. It should be noted that a strong spanwise component of velocity is generated, which is about 6 % of the streamwise component. This helps in the formation of streamwise oriented vortices which are essential in flow control.

The IR data under quiescent conditions are collected using FLIR camera and corrected with the surface emissivity of the actuator surface determined as 0.97. Due to reflection, only the dielectric

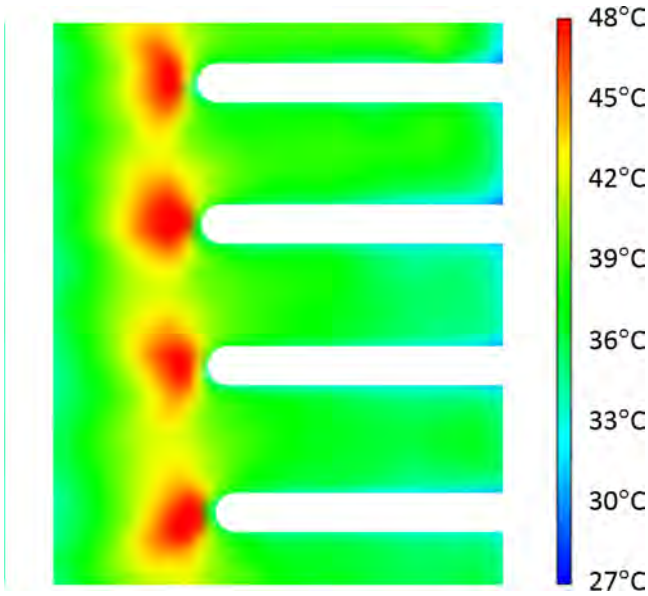

FIG. 5. IR image of the surface temperature around the serpentine actuator.

region is valid so we only showed the dielectric surface temperature. The final temperature data as plotted in Fig. 5 shows a maximum temperature of about 48°C at the tip of the fingers where incidentally the electric field is also the maximum. The surface temperature is within 30-35°C for the rest of the actuator. These temperature ranges may not have any significant effect on the flow field.

The flow visualization results for 30 mph (13.4 m/s) flow presented in Figure 7 show significant change in the trailing edge flow field. At higher speeds (> 30 mph) the flow visualization effect was harder to record due to lack of sufficient number of seeding particles. As compared to the baseline case with no plasma shown in Fig. 6(a), an approximate 30% reduction in size of the wake structure downstream of the trailing edge is observed in Fig. 6(b) when the serpentine actuator is turned on. This change is expected to positively influence the resulting wake drag.

The drag measurement procedure in the wind tunnel is as follows. First, data logging from the force balance are set to collect data for 60 seconds at a sampling rate of 10 Hz while the

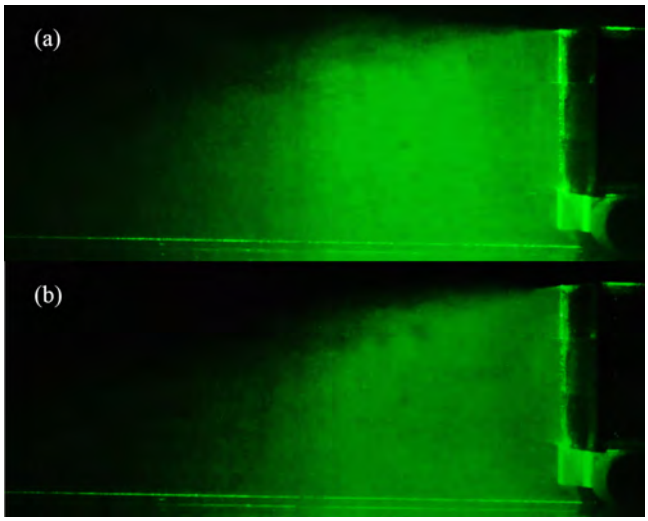

FIG. 6. Flow visualization at 30 mph. (a) Plasma off, (b) plasma on.

wind tunnel is running. Thereafter, the function generator is switched on to predefined voltage and frequency settings. After the function generator is switched off, the dynamometer continues to send force data to the computer for another 60 seconds. These 60-second buffers are used to ensure that the transient responses of the system do not affect the beginning or end of the sampled data. The buffer time also provides a good estimate of the baseline drag against which the change is referenced. For the straightedge (linear) actuator we only report drag results for two voltages, while for serpentine actuator we present data for a range of voltages. All plasma tests are done at 5 kHz for continuous mode using sinusoidal signal. For amplitude modulation (AM) mode a 125 Hz duty cycle is imposed over the continuous mode. Drag measurements for the linear and serpentine cases are plotted in Fig. 7. The collected data have been filtered digitally by a 1-D median filter with step size of 3 samples. The average error for drag force is within ±1% of the measured drag. Interestingly, in Fig. 7(a), the result shows a 5.1% increase of the measured drag using the linear actuator in continuous (Cont) mode at 60 mph (26.8 m/s) while in AM mode the drag increases by

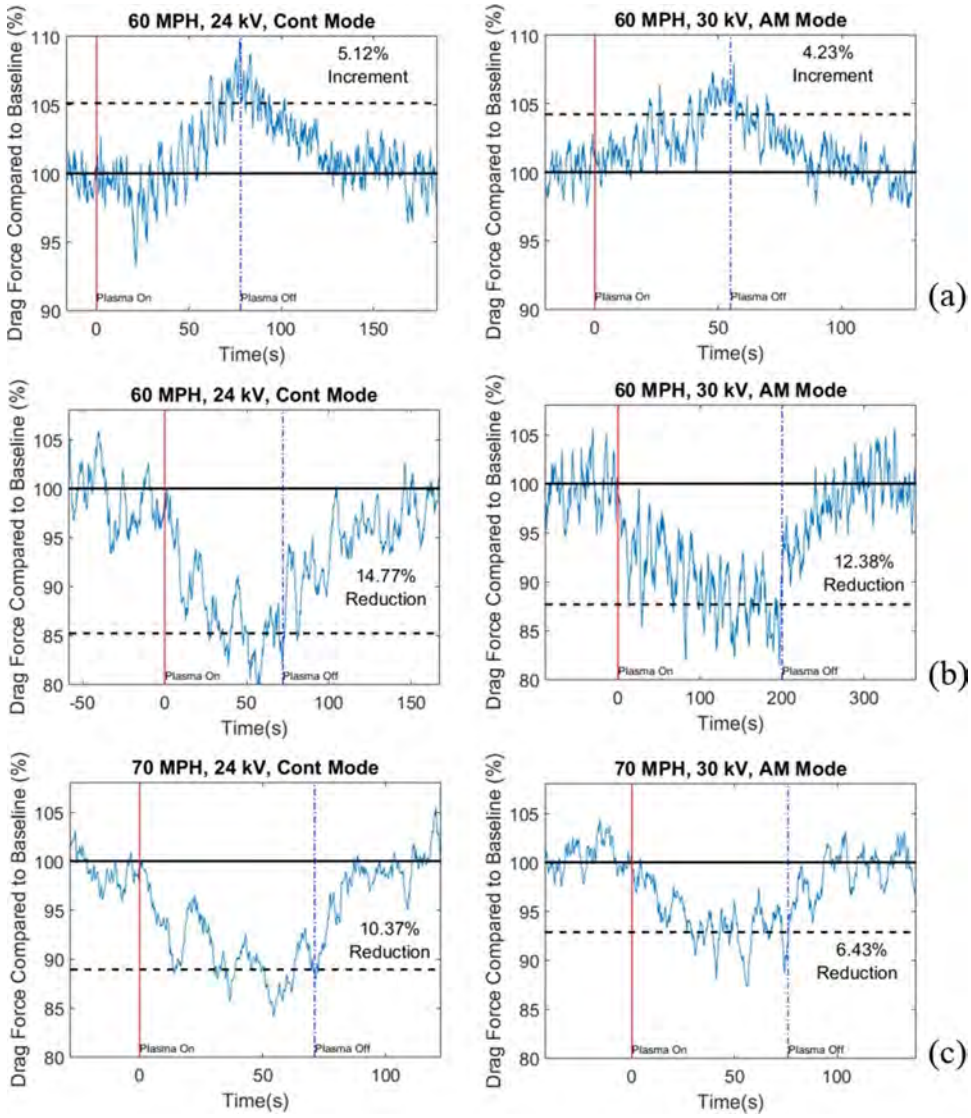

FIG. 7. Drag reduction performance comparison of plasma actuators with different input signals (a) linear actuators run for freestream velocity of 60 mph showing drag increase for both continuous mode and amplitude modulation mode. Serpentine actuators run for freestream velocity of (b) 60 mph (c) 70 mph.

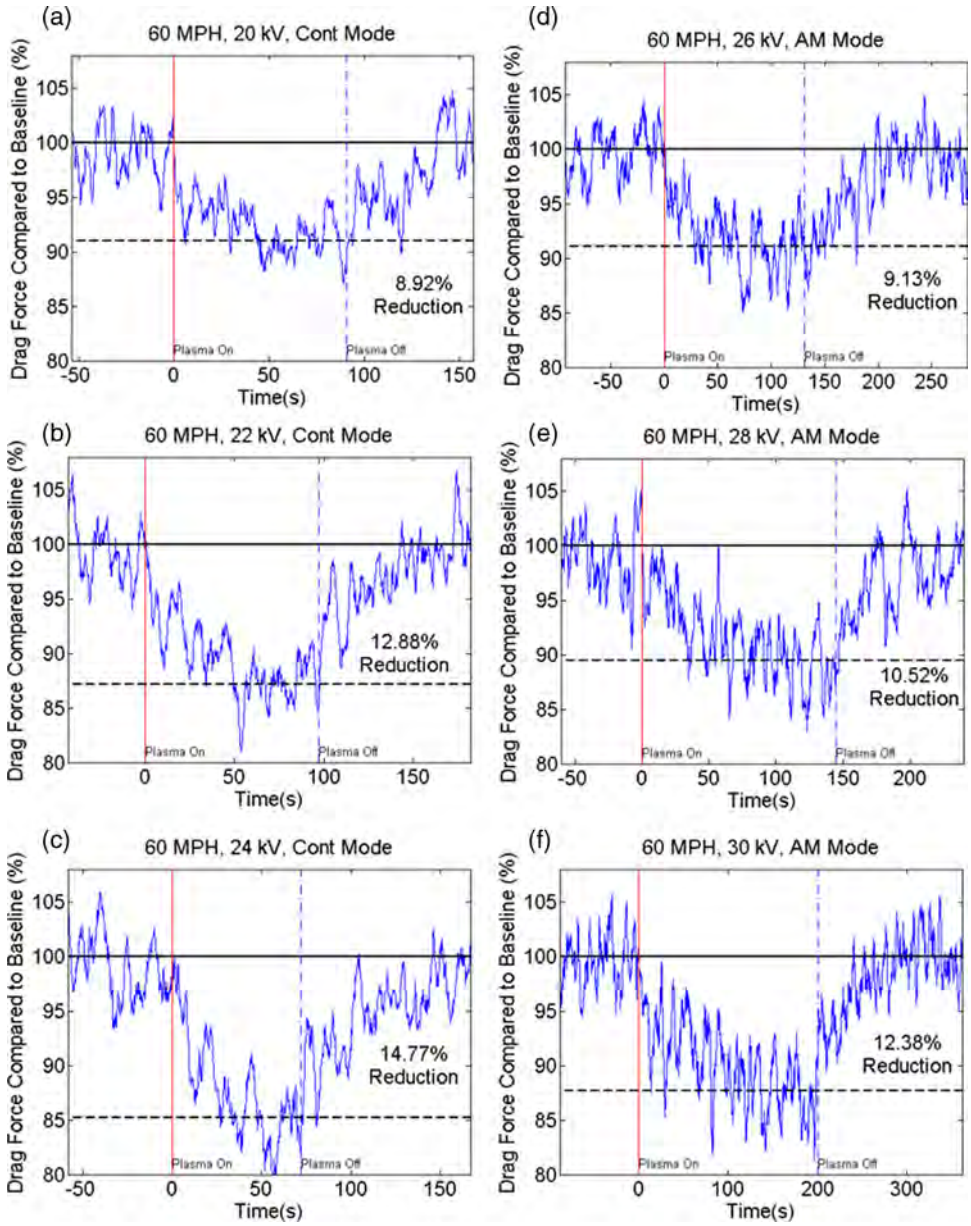

FIG. 8. Comparison of drag reduction performance for serpentine actuators at a freestream velocity of 60 mph with (a) - (c) Continuous mode and (d) – (f) AM mode.

4.2%. In comparison, serpentine actuator result shown in Fig. 7(b) documents a reduction in drag by 14.8% at 60 mph (26.8 m/s) and 10.4% at 70 mph (31.3 m/s).

Fig. 8 shows the drag reduction comparison between AM mode and continuous mode for different voltages at 60 mph. For the continuous mode and the AM mode the drag reduction % increases as the voltage goes higher. The slope of increase in drag reduction % from 20 kV to 22 kV is much higher than from 22 kV to 24 kV for the continuous mode. However the AM mode shows the same slope of increase. Since the actuators are located near the tail-end of the trailer covering less than 5% surface area, their resulting influence is assumed primarily on the wake drag behind the truck.

The drag measurements for the truck with the linear and serpentine actuators are compiled in Table I. Since we are only using one set of actuator just upstream of the tail end of the trailer, it is safe to assume that we are only influencing the pressure drag in the wake region of the trailer. Hence, a 14.8% reduction in total drag at 60 mph represents nearly 60% reduction of the wake drag,

TABLE I. Actuation performance comparison on drag reduction at a freestream velocity, V_{fs}.

V_{fs}	Voltage (Mode)	Linear Plasma Actuation	Serpentine Plasma Actuation
60 mph	20 kV_{pp} (Cont)		−8.9%
60 mph	22 kV_{pp} (Cont)		−12.9%
60 mph	24 kV_{pp} (Cont)	+5.1%	**−14.8%**
70 mph	24 kV_{pp} (Cont)		**−10.4%**
60 mph	26 kV_{pp} (AM)		−9.1%
60 mph	28 kV_{pp} (AM)		−10.5%
60 mph	30 kV_{pp} (AM)	+4.2%	−12.4%
70 mph	30 kV_{pp} (AM)		−6.4%

which is significant. It is important to point out that we have tested the comb-shaped serpentine actuator geometry with double the wavelength (results not shown for brevity) for which virtually no effect on the aerodynamic drag has been observed for flow speed above 30 mph. Based on our previous theoretical study,[16] the wavelength of the serpentine actuator is dependent on the flow parameters, namely, Reynolds number and flow streaks. As the free stream flow velocity increases smaller wavelength (reduced gap between the fingers) of the actuator becomes necessary to tune more flow streaks. Using a wavelength of around 400 wall units should be a good rule of thumb.[23]

Representative voltage and current information are plotted in Fig. 9. Specifically at 24 kV_{pp}, Fig. 9(a) shows the behavior of linear actuator while Fig. 9(b) shows that for serpentine actuator.

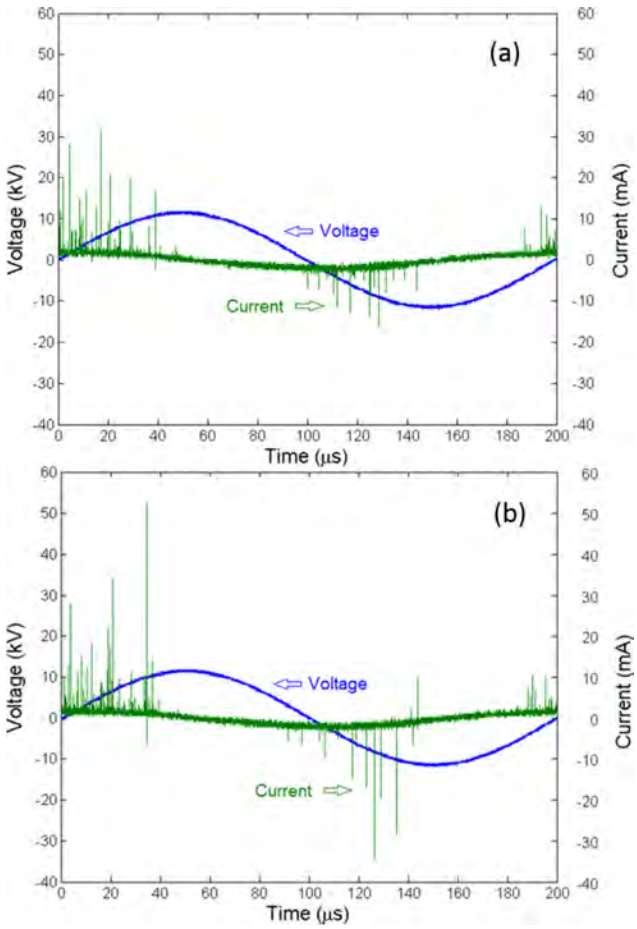

FIG. 9. Voltage and current behavior at 24 kV_{pp} as a function of time. (a) Linear actuation, (b) Serpentine actuation.

TABLE II. Power consumption data and full scale projection for serpentine actuator.

	Measured power for Truck Model	Scaling factor	Estimated power for a full scale truck
Electrical Power, P_{elec}	7.1 W	1:60 (1:l)	~425 W
Drag power reduction, P_{drag}	1.5 W	1:3600 (1:l^2)	~5400 W
Saved Power P_{saved}	−4.6 W		~5000 W

The total actual power expended is 7.05 W for the linear actuator while that for the serpentine actuator is 7.12 W.

Finally, the power saving from drag reduction is calculated using $P_{saved} = P_{drag} - P_{elec}$, where P_{drag} is calculated using P_{drag} = Drag force reduction × Freestream velocity. The measured power spent P_{elec} for serpentine plasma actuation with 24 kV_{pp} at 5 kHz in continuous mode operating under 60 mph free stream air velocity is 7.1 W as given in Table II. Despite a 14.8% reduction, the drag related power reduction is only 1.5 W for this 1:60 truck model.

Relations between power saved (P_{saved}) and power spent (P_{elec}) are also investigated under different running modes. The power saving increases with the power spent as shown in Fig. 10. One can also notice that although the peak to peak voltage is higher for AM mode (Fig. 9), the power spent in AM mode is much lower than that of continuous mode. In Fig. 10, it is also shown that the actuator consumes 3.1 W to save 0.9 W of total drag with an AM input signal at 26 kV_{pp} while it consumes 4.3 W to reduce 0.9 W of total drag under a 20 kV_{pp} continuous input signal. From the data shown in Fig. 10, the average effectiveness of both running modes can be calculated as power saved per watt power spent. For the AM signal, the average effectiveness is 2.7%, while with the continuous signal it is 2.1%.

While this may be discouraging, the following first order estimation for a full scale truck may be promising. As mentioned before, majority (>90%) of the aerodynamic drag for truck is due to pressure drag, i.e., frontal, gap, undercarriage and wake drag. Adding more actuators on the long flat surfaces of the trailer may reduce the skin friction drag, but will severely penalize the net power budget, as skin friction is a tiny fraction (<10%) of the total aerodynamic drag. Hence for practicality, we will only consider using a single set of serpentine plasma actuators just upstream of the edge of the trailer. Under this consideration and assuming that the truck coefficient of drag, c_d and the actuator effectiveness essentially remains constant with scale, the electrical power consumption

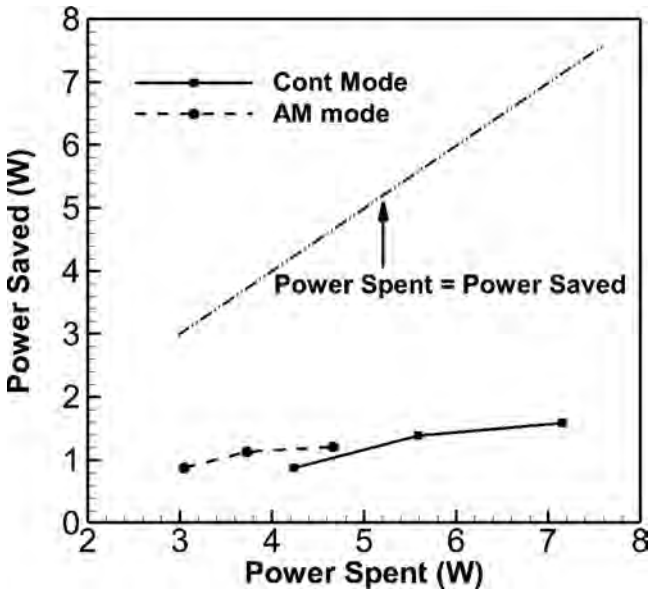

FIG. 10. Relation between power consumption and power spent under continuous and AM mode.

should scale up with the length of the actuator (1:60) while the drag power reduction should scale with the surface area (1:3600). Thus, for full scale truck the electrical power consumption of the actuator and the drag power reduction are estimated to be about 425 W and 5400 W, respectively, (see Table II). Note that one may also use another set of serpentine actuators just upstream of the tail end of the tractor for potentially further reducing pressure drag caused by unfavorable flow pattern around the gap. Even then the total electrical power consumption will be less than 20% of the amount of drag power reduced.

IV. CONCLUSION

We demonstrated reduction of aerodynamic drag for a scaled tractor-trailer model at 60 mph and 70 mph using serpentine dielectric barrier discharge actuator. While a comparable size linear plasma actuator fails to modify the drag at these speeds, a specific serpentine actuator arrangement tuned to flow streaks reduced the total aerodynamic drag by nearly 15% at 60 mph and over 10% at 70 mph air flow in a wind tunnel. Additionally, we also showed that the actuator can save 2.7 % total drag average per watt power consumed with AM input signal and save 2.1% total drag average per watt with continuous input signal. We note that more work needs to be done to explore the control possibilities of such actuation mechanism. The electrical power expended to run the actuator was 4.5 times more than the power saved by reducing the drag of this small tractor-trailer model. A simple scaling analysis showed the need for a detailed study to ascertain any practical possibility of reasonable energy savings for full scale ground vehicles.

ACKNOWLEDGEMENTS

Authors gratefully acknowledge partial support from Florida High Tech Corridor and Cool Flow Dynamics.

[1] M. Riherd and S. Roy, J. Phys. D: Appl. Phys. **46**, 485203 (2013).
[2] A. Washburn, "NASA's current plans for ERA airframe technology," 48th AIAA Aerospace Sciences Meeting, Orlando, FL (2010).
[3] J. R. Roth, D. M. Sherman, and S. P. Wilkinson, AIAA Journal **38**(7), (2000).
[4] S. P. Wilkinson, "Investigation of an oscillating surface plasma for turbulent drag reduction," 41st Aerospace Sciences Meeting and Exhibit, AIAA, Reno, NV, AIAA 2003-1023 (2003).
[5] E. Moreau, J Phys D- Appl Phys **40**, 605 (2007).
[6] J. R. Roth, Physics of Plasmas **10**(5), (2003).
[7] J. Huang, T. C. Corke, and F. O. Thomas, AIAA Journal **44**(1), (2006).
[8] J. R. Roth, D. M. Sherman, and S. P. Wilkinson, "Boundary layer flow control with a one atmosphere uniform glow discharge surface plasma," AIAA Meeting (Reno, USA, January 1998) paper #98-0328.
[9] T. C. Corke, C. L. Enloe, and S. P. Wilkinson, Annual Rev Fluid Mechanics **42**, 1 (2010).
[10] F. O. Thomas, T. C. Corke, M. Iqbal, A. Kozlov, and D. Schatzman, AIAA Journal **47**(9), (2009).
[11] M. Forte, J. Jolibois, J. Pons, E. Moreau, G. Touchard, and M. Cazalens, Experiments in Fluids **43**, 917 (2007).
[12] R. Durscher and S. Roy, J Phys D- Appl Phys **45**, 035202 (2012).
[13] S. Roy and C.-C. Wang, J Phys D- Appl Phys **42**, 032004 (2009).
[14] M. Riherd and S. Roy, J Appl Phys **114**, 083303 (2013).
[15] M. Riherd and S. Roy, J Phys D- Appl Phys **47**(12), 125203 (2014).
[16] R.J. Adrian and R. J., "Hairpin vortex organization in wall turbulence," Physics of Fluids **19**, 041301 (2007).
[17] R.M. Wood, A discussion of a heavy truck advanced aerodynamic trailer system. Presented at Int. Symp. Heavy Veh. Weights Dimens., 9th, University Park, PA (2006).
[18] H. Choi, J. Lee, and H. Park, Annu. Rev. Fluid Mech. **46**, 441–68 (2014).
[19] J. Patten, B. McAuliffe, W. Mayda, and B. Tanguay, NRC-CNRC Technical report no. CSTT-HVC-TR-205, (2012).
[20] K.-S. Choi, T. Jukes, and R. Whalley, Phil Trans R Soc A **369**, 1443–1458 (2011).
[21] P. Sujar-Garrido, N. Benard, E. Moreau, and J. P. Bonnet, Experiments in Fluids **56**, 70 (2015).
[22] H. Zare-Behtash, K. Kontis, and S. Roy, "Flow Control at Subsonic Speeds using Serpentine Plasma Actuators," in *45th AIAA Plasmadynamics and Lasers Conf*, AIAA-2014-2812 (2014).
[23] W. Schoppa and F. Hussain, Phys. Fluids **10**(5), 1049-51 (1998).